Mass Distributions of Coated Vesicles Isolated from Liver and Brain: Analysis by Scanning Transmission Electron Microscopy

ALASDAIR C. STEVEN,* JAMES F. HAINFELD,§ JOSEPH S. WALL,§ and CLIFFORD J. STEER‡

*Laboratory of Physical Biology and ‡Laboratory of Biochemistry and Metabolism, National Institute of Arthritis, Diabetes, and Digestive and Kidney Diseases, National Institutes of Health, Bethesda, Maryland 20205; and §Biology Department, Brookhaven National Laboratory, Upton, New York 11973

ABSTRACT Populations of coated vesicles purified from bovine brain (BCV) and from rat liver (LCV) have been characterized with respect to the parameters of mass and diameter by analysis of scanning transmission electron micrographs of unstained specimens. Coated vesicles from both sources are heterogeneous, particularly in their masses. The respective distributions, compiled from mass measurements of many individual particles, are complex and markedly different. BCV range from 20 Mdaltons to ~100 Mdaltons with a weighted average of 35 Mdaltons: most BCV (80%) lie between 20 and 40 Mdaltons, including peaks at ~26 Mdaltons and at ~34 Mdaltons. In contrast, LCV masses tend to be substantially higher, ranging from 20 to 220 Mdaltons with a weighted average of 66 Mdaltons. There is a prominent subpopulation at ~35 Mdaltons, and 59% of all LCV belong to a broad peak between 50 and 120 Mdaltons. The Kolmogorov-Smirnov distribution-free test was used to affirm the statistical reproducibility of these isolates. BCV diameters vary from 50 to 90 nm, and those of LCV from 50 to 150 nm. Both protein compositions, determined by SDS PAGE, are dominated by clathrin and they are generally similar, except that corresponding secondary bands, notably the clathrin-associated light chains, appear to have lower molecular weights in the case of LCV. From consideration of the joint mass-diameter distribution, it is apparent that coated vesicles of a given diameter vary considerably in mass and that this variation is due primarily to widely differing amounts of material enclosed within the clathrin coat.

Coated vesicles (CV)[1] are particulate cellular components that have drawn increasing interest in recent years (1, 2) not only because of their abundance and ubiquity, but also on account of the extensive range of intracellular functions in which they are thought to participate. In particular, they have been implicated in a variety of shuttling processes, including intracellular membrane transfer (3, 4), receptor-mediated endocytosis (5, 6), and plasma membrane recycling (7), as well as transport of materials destined for exocytosis (8). CV are spheroidal particles whose distinguishing feature, no matter where they occur, is their coat—a remarkable surface lattice of protein molecules that encases a globular lipid/protein vesicle. Kanaseki and Kadota (9) first described the hexagonal and pentagonal features of this coat. Subsequently, more detailed electron microscopy of isolated CV led to the proposal by Crowther et al. (10) that the coats are polyhedra that consist of a basic complement of 12 pentagons augmented by a variable number of hexagons. More recently, Heuser (11) has applied freeze-etching techniques to demonstrate graphically configurations of hexagons and pentagons in association with the fibroblast plasma membrane.

Current evidence suggests that the repeating structural unit of the CV surface lattice is the triskelion complex, which comprises three molecules of clathrin (M_r ~180,000), together with three light chains (M_r ~33,000), to give a molecular weight of ~0.64 Mdalton, with a sedimentation value of 8.4S (12). Hinged joints on the three triskelion legs have been

[1] *Abbreviations used in this paper:* CV, coated vesicles; STEM, scanning transmission electron microscopy; TMV, tobacco mosaic virus.

postulated to exist in order to facilitate packing of triskelions into closed polyhedra (13). Although the surface lattices of all CV characterized to date appear to be formed of triskelions, there is a marked variation in size among CV generally. An early paper by Friend and Farquhar (3) described two distinct populations in situ. One class, with diameters of >100 nm, was localized in the apical cytoplasm and attributed to involvement in endocytic processes. The other, with smaller diameters of ~75 nm, was found primarily in the Golgi region and was ascribed to participate in secretion. Other reports, based on electron microscopy of negatively stained CV isolated from various sources, indicate tissue-specific size ranges: e.g., human placenta, 70–120 nm (4); porcine brain, 45–60 nm (10); bovine adrenal medulla, 55–90 nm (10); chick oocyte, 60–105 nm (14); a murine lymphoma cell line, 100–120 nm (15). From these and other observations (see references 1, 2, 16), it can be concluded that although an extensive size range is encountered among CV generally and variation occurs even within single cells (3), the size ranges present in particular cell types are specifically regulated. Thus, elucidation of the factors that control the assembly of CV and the recycling of clathrin would appear to be an essential aspect of understanding their functions in cells. Moreover, systematic characterization of particular CV populations would seem a prerequisite for understanding the mechanisms that regulate particle size.

Hitherto, such information has been obtained primarily from electron microscopy of thin sections of in situ populations and by negative staining of isolated fractions of CV. However, the degree to which distinct components can be distinguished in mixed CV populations by either technique is limited: studies of thin sections have been constrained by rather low resolution, as well as by the ambiguity in determining diameters that arises from the (unknown) level at which the sectioning plane traverses any given particle. With negative staining, the limitations derive both from distortions effected by partial flattening (10, 17) and from non-uniformity in the modes of staining realized among different particles. Moreover, indirect methods such as analytical ultracentrifugation or x-ray diffraction are severely handicapped in regard to mixed populations of particles with a potentially high degree of polydispersity, although an average mass of 28 Mdaltons has been estimated from a sedimentation value of 220S for CV from porcine brain (10).

In this report we present analyses of the distributions of masses and diameters within two populations of purified CV, effected by scanning transmission electron microscopy of unstained specimens. Mass determinations of individual particles can be readily performed from such micrographs because the dark-field signal recorded in such an image is directly proportional to the mass in the represented portion of specimen. Similarly, measurements of projected diameter can be obtained without complications related either to sectioning properties or staining effects. In this way, we have characterized CV purified from bovine brain and from rat liver. The findings are discussed with particular emphasis on potential size-determining interactions between clathrin molecules and membrane components.

MATERIALS AND METHODS

Purification of CV: CV were isolated from rat liver according to previously described methods (18) as modified by Nandi et al. (19). In a typical preparation, done at 4°C, 1,000 g of liver (from ~100 200–250 g, fed, Sprague-Dawley rats) was homogenized with an equal volume of buffer A containing 0.1 M 2-*N*-morpholino-ethanesulfonic acid (MES, pH 6.5), 1 mM EGTA, 0.5 mM $MgCl_2$, and 0.02% (wt/vol) sodium azide in a Waring blender (four 10-s bursts) at maximum speed, according to the procedure initially described by Pearse (20). The homogenate was centrifuged for 45 min at 16,000 *g* (10,000 rpm in a GSA rotor [Sorvall/DuPont, Wilmington, DE]), and the resulting well-demarcated supernatant (~1,000 ml) was collected and centrifuged at 100,000 *g* (34,000 rpm in a Beckman 35 rotor [Beckman Instruments, Inc., Palo Alto, CA]) for 80 min. Each pellet was resuspended in 20 ml of buffer A using 18 strokes of the type A Dounce homogenizer. The suspension was brought to a total volume of 500 ml and centrifuged at 12,000 *g* (10,000 rpm, SS-34 rotor [Sorvall/DuPont]) for 10 min. The supernatant was carefully removed and centrifuged at 130,000 *g* (37,000 rpm, Ti 45 rotor [Beckman Instruments, Inc.]) for 80 min. The pellets were resuspended in homogenization buffer with the Dounce to give a total volume of 300 ml. After a low-speed centrifugation (10,000 rpm, 10 min) to remove aggregated material, the homogenate was centrifuged again at 130,000 *g* for 80 min, the supernatant was aspirated, and the pellets resuspended in 80 ml of buffer A, with 25 strokes of the Dounce. After another low-speed centrifugation, 6-ml aliquots of the CV-enriched suspension were layered onto 5–6 ml of a 17% sucrose-D_2O solution maintained at proper pH with the same buffer salts as in buffer A. These step gradients were centrifuged at 125,000 *g* (32,000 rpm in Beckman SW40 or SW41 rotors [Beckman Instruments, Inc.]) for 120 min at 16°C with the brake off. The supernatants were gently aspirated and the surface of the pellets washed with 2-ml aliquots of buffer A. These pellets containing the CV were resuspended in buffer A using 25 strokes of the Dounce. After centrifugation at 12,000 *g* for 10 min to remove aggregated material, the CV were stored at 4°C at a concentration of 2–3 mg/ml until needed. The CV were used within 2 wk of preparation and were stable over at least this period, as judged by gel electrophoresis and electron microscopic observations. The yield from a typical preparation contained ~40 mg of protein.

Coated vesicles from bovine brain were isolated according to the method of Nandi et al. (19). After the pia and white matter of the brains were removed, the gray material was homogenized 1:1 in buffer A and centrifuged in the GSA rotor at 16,000 *g* (10,000 rpm) for 45 min. The suspension was purified by using similar high-speed (60 min) and low-speed (10 min) centrifugations of the homogenate as described above. The final 8% sucrose-D_2O step gradients were centrifuged at 125,000 *g* (32,000 rpm in the SW40 and 41 rotors) for 120 min at 16°C with the brake off. The CV-containing pellets were washed with 2-ml aliquots of buffer A and stored in 1–2 ml of the buffer until needed. CV stored in pellet form showed no evidence of change either morphologically or in terms of protein composition over a 2-wk period. The yield from a typical preparation, starting with 1,500 g wet wt of brain, contained ~90 mg of protein.

Analytical Gel Electrophoresis: Proteins were subjected to electrophoresis in SDS polyacrylamide slab gels as described by Laemmli (21). Aliquots of 100–120 μg protein were electrophoresed through an 8.5% separating gel and a 4% stacking gel. Separation of the subunits was carried out overnight at room temperature, with constant current (20 mA). Gels were stained with 0.15% Coomassie Brilliant Blue R-250 in a mixture of 10% acetic acid and 50% methanol. Gels were calibrated with the following molecular weight standards: myosin, 200,000; β-galactosidase, 130,000: phosphoylase B, 94,000; bovine serum albumin, 68,000; and ovalbumin, 43,000 (cf. Fig. 1). Protein determinations were done according to the method of Lowry (22) with bovine serum albumin as standard.

Photographic records of stained gels were scanned with a Perkin-Elmer (South Pasadena, CA) 1010G scanning microdensitometer (23) using 100-μm apertures and a 100-μm sampling interval. The resulting digital data were analyzed by means of the PIC (24) and MLAB (25) systems of computer programs, implemented on PDP 11/70 and DEC-10 computers (Digital Equipment Corp., Marlboro, MA), respectively. To enhance the visibility of minor bands, the gels were overloaded with the result that the linear range of the recording film (type 4162; Eastman Kodak Co., Rochester, NY) was exceeded with respect to the clathrin band. Accordingly, the data were subjected to a nonlinear mapping to compensate for this effect before further analysis. The baseline was determined by a linear regression through the lowest-density points of the laterally averaged trace, and the overall fractions of clathrin and light chains were determined by two-dimensional integration of the appropriate regions of the gels.

Confirmation that these experimental conditions remained within the linear region for dye-binding by clathrin was established according to the method of Fenner et al. (26), using purified clathrin.

Conventional Electron Microscopy: Preparations of CV were examined by conventional transmission electron microscopy using a Philips (Mahwah, NJ) EM400T electron microscope operating at 80 kV. A liquid

nitrogen cold trap was used routinely. After adsorption to a thin layer of evaporated carbon supported on a collodion film substrate, specimens were washed (two cycles) with 20 mM Tris-HCl, pH 7.0, and stained with a 1% aqueous solution of uranyl acetate. After 10 s, excess fluid was wicked off with filter paper and the grid was allowed to air-dry.

Scanning Transmission Electron Microscopy (STEM): STEM was carried out at the Brookhaven Biotechnology Resource (27) with the 40-keV electron probe focused to 0.25 nm diam. Images were recorded directly in digital form, with parallel acquisition of two dark-field images (each (512 × 512 pixels) in the small-angle (15–40 mrad) and large-angle (40–200 mrad) detectors, respectively. However, only the large-angle signal was used for mass analysis: its quantum collection efficiency is ~40% and its detection efficiency is ~100%. Specimens were maintained at −130°C on the liquid N_2-cooled stage during observation.

Unstained specimens were prepared by freeze-drying at a constant sublimation rate over a period of 6–8 h according to previously described procedures (28), except as detailed below. To avoid overlaying specimens with a film of protein denatured at the air-water interface, the drop-injection technique (29) was used throughout. A drop (2.5 μl) of coated vesicle suspension at 100–200 μg/ml total protein in buffer A (cf. above) was injected into a 2.5-μl drop of distilled H_2O previously applied to the grid. The substrate was a carbon film (~2.5 nm in thickness on average) supported on a fenestrated thick-carbon support, which had previously been glow-discharged in N_2. After 5 min, the grid was washed five times with drops of 10 mM ammonium acetate (pH 6.5); then tobacco mosaic virus (TMV) reference particles were added and the freeze-drying protocol was completed as described (28). The spatial distribution of particles on grids prepared in this manner was notably uniform and reproducible.

Mathematical and Statistical Analyses of Data: The masses of individual particles were determined using both the Brookhaven computational system (30) and the PIC system (24). Repeated measurements of the same particles confirmed that these systems yield consistent results. Backgrounds were determined locally as described (30, 31). Mass values were calibrated relative to the average linear density obtained for the TMV particles present in a given micrograph. CV masses were determined from micrographs whose fields of 512^2 pixels covered (1.04 μm^2) or (2.08 μm^2).

Mathematical quantitations, most statistical procedures, and all computer graphics were carried out using the MLAB package (25) on a DEC-10 computer, in coordination with a model 4012 graphics terminal (Tektronix, Inc., Beaverton, OR). The Kolmogorov-Smirnov distribution-free test (32) was performed using a program written for this purpose, incorporating a subroutine obtained from the IMSL utility library (IMSL, Inc., Houston, TX).

RESULTS

Comparative Protein Compositions of BCV and LCV

CV populations isolated from bovine brain and from rat liver were analyzed by SDS PAGE to compare their respective protein compositions (Fig. 1). In both cases, the predominant component was clathrin, as expected from earlier reports (14, 18, 20). From quantitative digital analysis of stained gels (Fig. 1), we estimated clathrin to account for 51 (BCV) and 39% (LCV) of the total protein in these preparations. The patterns of secondary bands were qualitatively similar in the two cases, except that corresponding bands were generally displaced towards lower molecular weights in the LCV preparations (cf. Fig. 1). For example, the light-chains that remain in association with clathrin upon uncoating CV, and which are thought to participate with clathrin to form triskelion complexes (33, 34), appeared to consist of two bands in both cases. These have apparent molecular weights of ~36 and 33 kdaltons for BCV (together 6.7% of total protein), compared with ~33 and 30 kdaltons for LCV (together, 5.3% of total protein). Similarly, the LCV proteins, which seem to correspond to the "110K" (35) proteins of BCV, average only ~96 kdaltons. Of the bands present on the LCV track to which there are no obvious counterparts for BCV, the most conspicuous are a group in the range of 65–75 kdaltons, and a less prominent component at ~40 kdaltons.

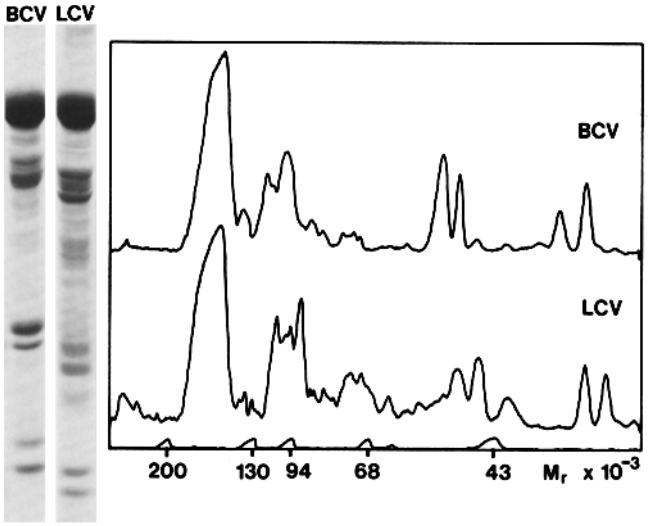

FIGURE 1 SDS PAGE of purified coated vesicle populations isolated from bovine brain (*BCV*) and from rat liver (*LCV*). Photographic records as well as densitometric scans compare the protein compositions of the respective isolates. In both cases, the major component is clathrin (M_r ~180,000), but differences are apparent between the respective distributions of secondary bands (cf. Results).

STEM of Unstained Coated Vesicles

Typical dark-field STEM images of unstained LCV and BCV are shown in Fig. 2. For reference, a bright-field CTEM image of BCV contrasted by negative staining with uranyl acetate is also included (Fig. 2*c*). The unstained CV were prepared for electron microscopy by freeze-drying, after repeated washing with dilute solutions of ammonium acetate, a volatile salt. This procedure evolved as an effective way to minimize residual salt deposits while preserving the structural integrity of the CV by maintaining buffering during the wash cycles. Biological material per se is more sensitive to radiation damage than are distributions of heavy metal stain, so electron irradiation levels were kept to a minimum and all analyses were performed on first-scan images recorded with average doses of 70–300 electrons/nm^2. As a further measure to foster preservation of structure, all specimens were maintained at a temperature of about −130°C during observation to inhibit the diffusion of radiation products and to eliminate contamination.

From visual inspection of these images, it was immediately apparent that the CV are heterogeneous, in terms both of physical dimensions and of cumulative image intensity (electron scattering power). This property applies to both types of CV (Fig. 2) and it is particularly evident for LCV, among which the incidence of larger particles is also clearly higher. From these observations, it was also evident that the preparations of CV particles were indeed highly purified. Among the BCV, identifiable contaminants amounted to a few non-coated vesicular particles (e.g., *U* in Fig. 2, *a* and *b*) which occurred at a frequency ~5% that of the BCV, and small amounts of reticular substance that presumably derived from the membranes of the source tissue.

On average, LCV are perceptibly larger and more massive than BCV (cf. Fig. 2). To judge by microscopy, they show a similar degree of purity to the BCV. However, LCV also contain particles that are apparently incomplete (e.g., *P* in

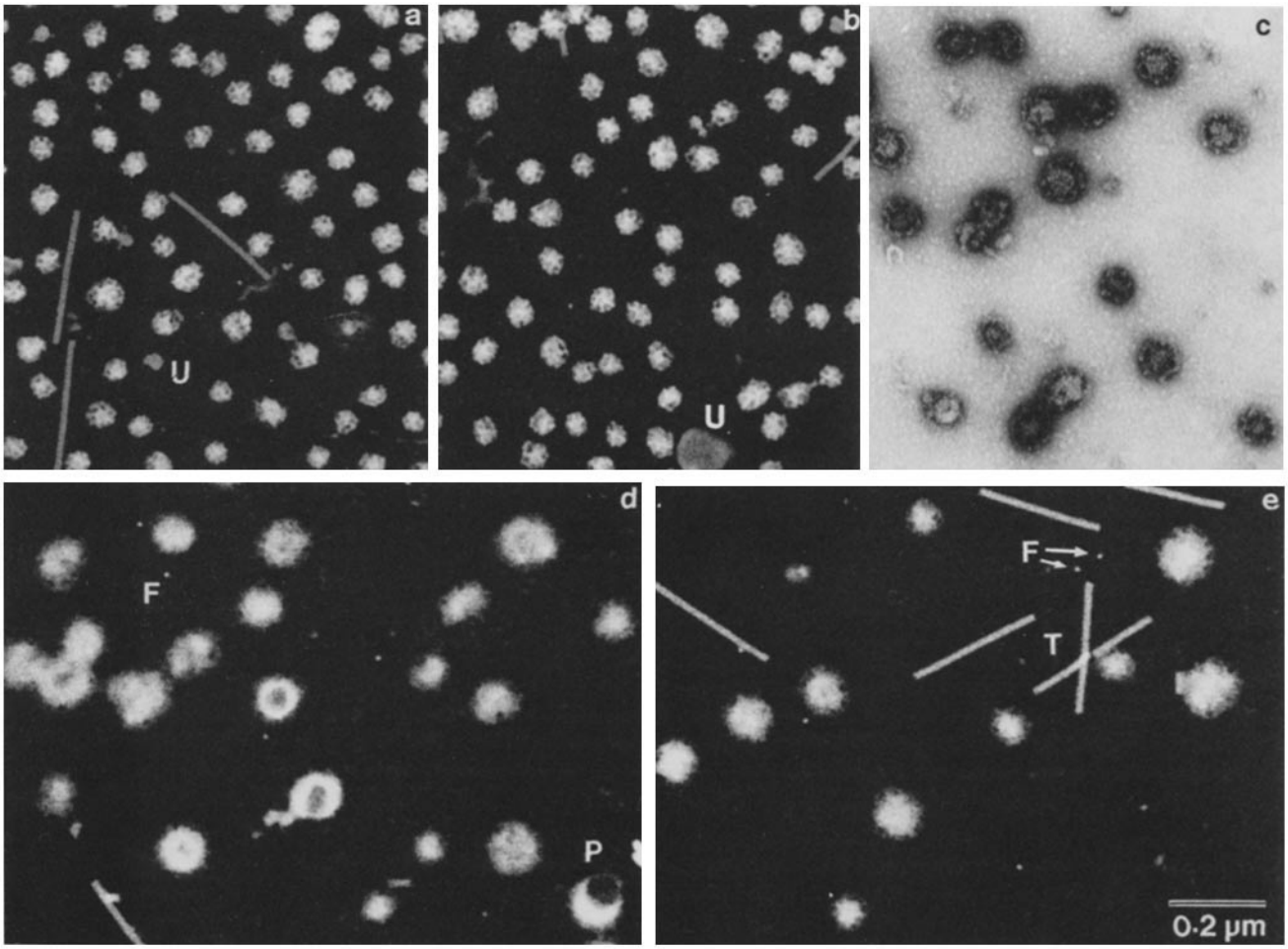

FIGURE 2 Electron micrographs of coated vesicles isolated from bovine brain (*a*, *b*, and *c*) and from rat liver (*d* and *e*). Unstained CV imaged in STEM dark-field mode, after preparation for electron microscopy by freeze-drying, are shown in *a*, *b*, *d*, and *e*. For comparison, a CTEM image (*c*) of BCV negatively stained with uranyl acetate is included. All micrographs are at the same magnification. The STEM dark-field images are reproduced so that the more massive features are white against a dark background (the carbon film substrate). These preparations appear to be highly purified, the most common impurities being (relatively infrequent) noncoated vesicles (*U*) of various sizes, which are easily distinguished from CV on morphological grounds. The rod-like particles (*T*) are tobacco mosaic virions, used as internal mass standards. Small dense-cored particles (*F*) are quite abundant in LCV preparations and we conclude that they most likely represent contaminating ferritin molecules (44) (cf. Results). Some of the larger LCV (e.g., *P*) have a nonsymmetrical appearance which is suggestive of incomplete assembly, or possibly, of damage.

Fig. 2*d*). These occur at the level of 10–15% of all particles, and are also observed, although less conspicuously, in conventional electron microscopy of negatively stained preparations. Although we cannot rule out the possibility that these may represent LCV that have become partially disrupted during the course of preparation, we consider this explanation of their origin to be unlikely because such particles are rare among BCV isolated in a similar manner. An alternative possibility is that they may represent coated pits extracted as a result of tissue homogenization before they could mature into CV.

The STEM dark-field signal is proportional to the mass present in a given portion of specimen sampled by the electron probe (36, 37), at least over the dynamic range spanned by these images (cf. Appendix). This property facilitates the determination of mass of individual particles by integrating the cumulative signal from a designated area of the image (which contains the particle of interest), after effecting a background subtraction. We have performed many such measurements for both BCV and LCV. The results are presented in Fig. 3 and Table I. The criteria for selecting a given CV for a mass measurement were as follows: (*a*) it should be apparently intact; (*b*) it should be surrounded by a clean, uniform, tract of carbon film; (*c*) the periphery of the particle should be unambiguously distinguishable (e.g., the particles should not be clustered). All CV meeting these criteria were measured, so that the resulting distributions probably represent unbiased samplings of the respective purified populations. Since all CV, of whatever size, are encased in clathrin, differential adsorption to the substrate is unlikely to exercise any bias in favor of specific size classes.

Distributions of Molecular Weights of BCV and LCV

The respective distributions of molecular weights, compiled from many hundreds of individual measurements, are plotted in Fig. 3. These distributions are complex and characteristically different. To interpret them, it is first necessary to consider the uncertainty implicit in an individual measure-

ment. It is a basic property of STEM mass measurements that they become progressively more precise with increasing mass of the particles measured (27, 38). A formalism has been derived that yields the fractional experimental error in a mass measurement caused by random fluctuations in the thickness of the carbon substrate, and by shot noise arising from the finite electron dose (28). Under the experimental conditions used here, an error of 0.3% is to be expected for a CV of 40 Mdaltons. However, the CV data are all normalized relative to the local average of TMV particles, and a standard deviation of 2.5% is characteristic of the set of TMV particles present in a given micrograph analyzed in this study. In practice, other sources of uncertainty arise, which mainly relate to the efficacy of the experimental procedures used to eliminate extraneous biological matter and salt deposits while maintaining the structural integrity of individual particles (31, 39). The standard deviation of repeated measurements of the same particles is at the 1–2% level. Thus, we estimate the experimental uncertainty for any given CV mass measurement to be of the order of 3%, with the TMV calibration contributing the major source of error. The relative masses of CV present in a given field are determined somewhat more precisely.

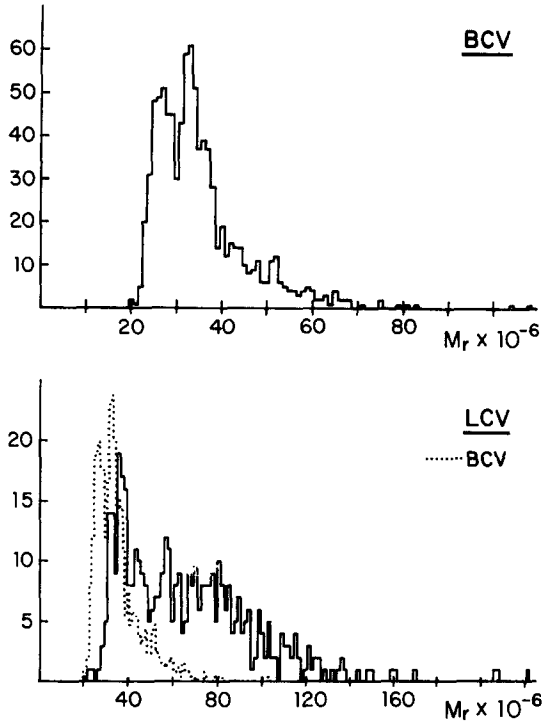

FIGURE 3 Histograms describing the distributions of particle masses encountered in purified populations of BCV (n = 904) and LCV (n = 442).

Distribution of BCV Masses

The minimum molecular weight for BCV is ~20 Md, and the majority of these particles (75–85%) have masses between 20 and 40 Mdaltons (Fig. 3). In this range, the distribution appears to contain two peaks at ~26 and 34 Mdaltons, respectively, although the degree of heterogeneity among different particles is much greater than twofold, even within this interval. The remainder have higher masses, generally ranging up to ~80 Mdaltons and averaging 51 Mdaltons, but a few BCV have masses as high as 108 Mdaltons. The weight average over the entire distribution is 35 Mdaltons. In each of the four preparations analyzed, the mass limits bounding the major component of the distribution, viz. 20 and 40 Mdaltons, were clearly and reproducibly defined. The rather dispersed distribution of the remaining particles was also similar in each case, although the overall fraction of BCV with masses in excess of 40 Mdaltons varied slightly among different preparations, in the range 15–25% (cf. Table II).

Distribution of LCV Masses

The minimum molecular weight encountered in these preparations was also 20 Mdaltons, but the LCV range extends at least as high as 220 Mdaltons. There is a prominent subclass of LCV with masses around 35 Mdaltons, similar to one of the classes observed among BCV. However, the major part (59%) of the total LCV distribution lies in a broad peak between 50 and 120 Mdaltons. The global weight-average LCV mass is 66 Mdaltons.

The major statistical parameters of the respective distributions are summarized in Table I. These results emerged consistently from repeated mass analyses. Because the results of such experiments are defined only in a statistical sense, their reproducibility was established by comparing various subdistributions of mass measurements according to the Kolmogorov-Smirnov test (32). This test provides a quantitative measure of the probability that two sets of measurements will both represent samplings of the same underlying distribution, or that they will derive from significantly different distributions. For present purposes, this test has the advantage of being independent of the shapes of the distributions involved. The results obtained by comparing the outcomes of STEM analyses of independently obtained isolates of BCV and LCV, and of repeated microscopic analyses of given preparations are presented in Table II.

These analyses have established (*a*) that CV preparations from both brain and liver are highly heterogenous, (*b*) that these populations are reproducible in the sense of statistical distributions, and (*c*) that these distributions are characteristically different. The possibility was considered that the use of a 17% sucrose-D_2O step gradient to isolate purified LCV, as opposed to a 8% sucrose-D_2O at the corresponding stage

TABLE I

Molecular Weight Distributions of Isolated CV: Statistical Parameters

Source tissue	Bovine brain	Rat liver
Mdaltons		
Observed range	19.1–107.9 (n = 904)	21.5–220.2 (n = 442)
Weighted average	34.7	66.1
Deciles	24.6/26.5/28.4/30.7/32.3 34.0/36.3/40.5/49.0	34.1/37.8/44.4/53.5/61.1 70.1/78.3/87.7/103.7
Prominent subpopulations	23–29 (Mean = 26.3): 31% 30–38 (Mean = 33.6): 40%	28–39 (Mean = 34.7): 20% 50–120 (Mean = 76.8): 59%

TABLE II

Pairwise Evaluation of CV Mass Data Sets as Like/Unlike Samplings: Comparison According to Kolmogorov-Smirnov Distribution-free Test

Proposition	Conclusion	Sets of measurements compared*		Probability ($P < 0.05 \rightarrow$ significantly dissimilar)
		Data set A	Data set B	
Are the products of independent biochemical preparations of LCV statistically reproducible?	Yes	$n = 301$	$n = 142$	0.55
Are the products of different biochemical preparations of BCV statistically reproducible?‡	Yes	$n = 333$	$n = 154$	0.87
Are independent STEM mass analyses of a given LCV preparation reproducible?	Yes	$n = 344$	$n = 192$	0.29
Are independent STEM mass analyses of a given BCV preparation reproducible?	Yes	$n = 333$	$n = 191$	0.89
Are purified BCV significantly different from purified LCV?	Yes	$n = 904$	$n = 442$	10^{-45}
Are BCV pelleted through 17% sucrose-D_2O gradient significantly different from BCV pelleted through 8% sucrose-D_2O?	No	$n = 904$	$n = 314$	0.23

* In each of these tests, two sets of measurements (A and B) obtained from different experiments are compared. The number of measurements (n) in both sets are listed here.

‡ In some comparisons, the test results initially suggested that the data sets were different. Upon closer analysis, these results were found to originate from a slight variability between preparations of the fraction of BCV with masses in excess of 40 Md (cf. Fig. 3), viz. 15–25%. Tested separately, the two subpopulations (up to 40 Md and above 40 Md), were indistinguishable. We are not aware of the source of this small, but apparently significant, variability in the overall fraction of larger BCV: conceivably, it may be related to the age or nutritional state of the individual source animal.

§ The program used does not quantitate probabilities more remote than 10^{-4}.

of BCV purification, might result in selective retardation of less massive LCV and thus contribute to the observed differences between the respective populations. To test this proposition, we compared LCV isolated using both types of gradient by CTEM observation after negative staining. No differences between the samples was apparent in respect of CV sizes, although the pellet from the 8% gradient contained a much higher incidence of noncoated membrane vesicles and fragments. Similarly, BCV were also isolated using the 17% sucrose gradient, and upon STEM analysis, the resulting distribution of masses obtained was found to be unaffected by this change in experimental procedure (Table II). We therefore discounted this possibility as the source of the observed difference between the respective molecular weight distributions.

Variability in Diameter and Vesicular Contents of Coated Vesicles

In addition to the observed variations in mass, we also observed appreciable differences among the physical dimensions and shapes of these particles. For illustration, a gallery of STEM images of BCV of various masses and morphological appearances is presented in Fig. 4. The particles shown in Fig. 4, *g* and *h*, respectively, represent BCV that have closely similar dimensions, but whose masses differ radically on account of widely differing vesicular contents. In some of these images, e.g., Fig. 4, *b* and *c*, features of the clathrin surface lattice are visible with particular clarity.

The outer diameters of several hundred particles were determined by averaging, in each case, three measurements made at equal angular increments. To reduce uncertainties, spherically symmetrical particles were selected for this purpose. The resulting sets of coordinates (mass, diameter) are displayed in a two-dimensional plot in Fig. 5. Here LCV and BCV data are combined. When plotted separately, the respective distributions overlapped, and although the LCV data were generally displaced towards higher values of both param-

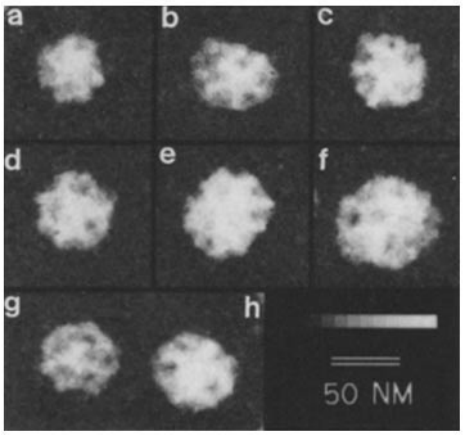

FIGURE 4 A gallery of STEM dark-field images of unstained BCV, uniformly normalized and displayed according to the grey-scale shown: the calibration ramp represents equal increments of density of 3.2 kdaltons/nm^2 and portrays one level below the average background value and eight levels above. These particles were selected to illustrate the range of variations in shape, morphology, dimensions, and mass encountered in BCV populations: (a) 24.3 Mdaltons; (*b*) 33.0 Mdaltons; (c) 41.4 Mdaltons; (*d*) 37.8 Mdaltons; (e) 56.8 Mdaltons; (*f*) 80.1 Mdaltons; (*g*) 26.2 Mdaltons; (*h*) 44.4 Mdaltons. *a* and *d* are representatives of the two prominent subpopulations detected in the overall distribution of BCV masses (cf. Results and Fig. 3).

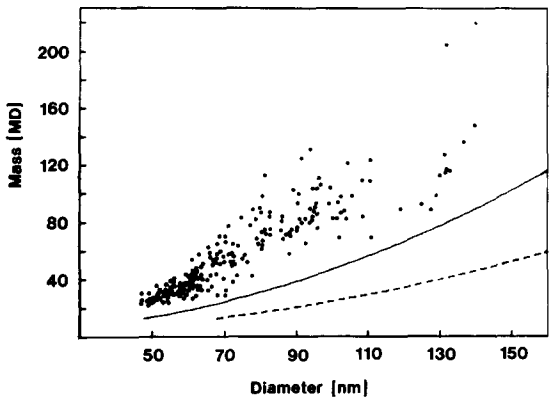

FIGURE 5 2-dimensional plot representing the joint mass/diameter distribution of CV. Both LCV (140 points) and BCV (113 points) were combined in this plot. The solid line represents the mass/diameter dependency which is to be expected for coats constructed from triskelions according to the geometrical scheme proposed by Crowther and Pearse (13) (cf. Results). The difference between the mass-coordinate of a given point and this curve gives an estimate for the internal mass of that CV (i.e., the mass contained within its coat). The eventuality that CV flatten to some extent upon adsorption to the carbon film substrate could affect these estimates of the surface lattice masses, by resulting in an overestimate of the surface lattice area. The dashed line represents the consequences of the most extreme case of flattening, in which particles are totally flattened, but spread so as to preserve their surface areas.

eters, there was no obvious way to distinguish between the respective distributions of points in the 25–50-Md range.

It seems probable that the variation in size among CV is associated with a corresponding variability in the clathrin coats arising from different polyhedral forms. Although we cannot determine precisely how many distinct polyhedra are represented in these populations, we can nevertheless estimate the mass fraction contributed by the triskelion surface lattice for a CV of any given diameter by calculating first the surface area of a sphere of that diameter and from that the number of triskelions required to cover it. To estimate the packing density of triskelions, we adopted the scheme proposed by Crowther and Pearse (13), according to which clathrin coats take the form of polyhedra consisting of 12 pentagons plus a variable number (n_h) of hexagons, and one triskelion is associated with each vertex of the polyhedron. The inter-vertex spacing was taken as 18.7 nm (13), and the triskelion mass as 0.64 Mdalton. Under these premises, the masses, $M(n_h)$, and the unflattened diameters, $D_u(n_h)$, of the resulting polyhedra are given by the equations:

$$M(n_h) = 1.28\ (n_h + 10)\ \text{Mdalton};$$

$$D_u(n_h) = (289 \cdot n_h + 2{,}298)^{1/2}\ \text{nm}.$$

The resulting mass-diameter curve is included in Fig. 5, and for any given CV represented in this plane, an estimate of the mass of its vesicular contents is given by the displacement of its mass coordinate above this curve. Thus, we estimate that overall the coats account for ~50% of the total BCV mass (sampling of 113 particles, average mass 37 Mdaltons) and ~30% for LCV (sampling of 140 particles, average mass 73 Mdaltons). For individual data points, the experimental errors are ~3% (i.e., 1–3 Mdaltons) in mass, and ~5% (i.e., 2–6 nm) in diameter. In view of these relatively small uncertainties, it is evident from Fig. 5 that CV of approximately the same size vary greatly in their masses and vice versa. To demonstrate this point more directly, we show a set of LCV images in Fig. 6. The diameters of these particles are very similar, 130–140 nm, but their masses are strikingly different, ranging from 85 to 186 Mdaltons. This variation appears to be due primarily to their differing contents. The particle of Fig. 6*c* represents an extreme case. Its content has a definitely bipartite appearance and may in fact represent two vesicles enclosed within the same clathrin shell.

DISCUSSION

In this study, we have exploited the electron optical advantages of STEM to obtain images of purified CV without recourse to contrast enhancement by heavy-metal staining or shadowing. From these images, the masses and diameters of many CV particles have been determined, and the overall distributions of CV particles purified from rat liver and from bovine brain, respectively, have been built up from these individual measurements. Pronounced variability is observed within both populations, although they are statistically well defined in the sense that our results are reproducible with respect to repeated electron-microscopic analyses of a given isolate, as well as for sets of measurements from separate isolates (Table II). From these images, we infer that these preparations have a low incidence of contaminants, which are primarily noncoated vesicular particles and small amounts of membranous debris. Unlike other biophysical methods for sizing microscopic particles (such as sedimentation analysis, light-scattering techniques, or x-ray diffraction), the STEM results would not be systematically affected by the presence of such contaminants, even in substantial amounts. However, the observed purity of the CV isolates is of importance when considering the observed differences between the physical parameters of BCV and LCV populations in light of their differing protein compositions (Fig. 1).

CV Structure and Protein Composition

The respective clathrin molecules of BCV and of LCV migrate indistinguishably on SDS gels, and there is general similarity between their respective patterns of secondary bands, except that LCV proteins tend to have systematically

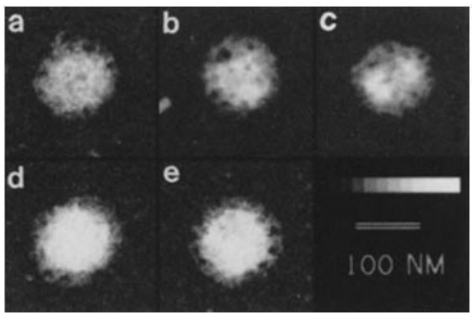

FIGURE 6 A gallery of STEM dark-field images of unstained LCV, uniformly normalized and displayed according to the given grey-scale: this calibration conveys equal increments in density of 3.3 kdaltons/nm^2. The average background level (i.e., average mass-thickness of the carbon film substrate) is the second darkest level. These particles were selected to illustrate the variation in mass among LCV, and in particular, the variability in their vesicular internal contents. These LCV all have outer diameters of ~135 nm: (*a*) 104 Mdaltons; (*b*) 95 Mdaltons; (*c*) 85 Mdaltons; (*d*) 186 Mdaltons; and (*e*) 169 Mdaltons.

lower molecular weights than their apparent BCV counterparts. The finding that LCV light chains are significantly different from those of BCV is intriguing in view of the report by Lisanti et al. (33) that these subunits are required to promote the assembly of clathrin into "baskets" in their in vitro system. In view of this observation of the modulation of clathrin assembly by such proteins, it is conceivable that different light chains might influence CV size distributions by favoring the assembly of particular sizes of coat. Alternatively, the respective clathrin molecules may differ in this respect. However, further work is required to clarify the status of this conjectural form-determining mechanism.

We estimate that clathrin constitutes ~39% of total Coomassie-stainable protein for purified LCV and ~51% for BCV in preparations that, to judge by electron microscopy of negatively stained samples and STEM of unstained specimens, contain only trace amounts of particulates other than CV. These data are somewhat higher than the earlier determination for BCV by Woodward and Roth (40) of 40% clathrin, but somewhat lower than the determination by Mello et al. of 64% clathrin (41). The reasons underlying these disparities are not obvious. However, one possible contributing factor might arise from the fact that the purification procedures used in these studies involved density gradient centrifugation with high concentrations of sucrose (cf. reference 20). Nandi et al. (19) have recently shown that such treatment leads to the separation of clathrin from membrane lipid, with the implication that CV populations so obtained may contain particles reformed out of breakdown products.

When the respective complements of light chains are taken into consideration, we reach figures of 44% (LCV) and 58% (BCV) for the biochemically derived estimates of the protein mass fractions contributed by the triskelion surface lattices. The determination of a somewhat smaller fraction of surface lattice protein for LCV than for BCV correlates plausibly with the larger average size of LCV, which confers a greater internal capacity per fixed amount of clathrin in this system. These figures are generally consistent with corresponding estimates of fractional surface lattice mass from electron-microscopic measurements (Fig. 5), where the surface lattice density of triskelions has been calculated from the packing principle put forward by Crowther and Pearse (13). However, this correlation is still somewhat tentative on account of the ambiguity that relates to the depth within the particle to which the 18.7-nm inter-vertex spacing determined from the negatively stained projection should apply, as well as to the eventuality of partial flattening upon adsorption of these particles to the carbon film. We hope that further studies will clarify these aspects.

Structural Variation among Coated Vesicles

The occurrence of size variation among CV particles, particularly in different tissue types, has been disclosed through earlier studies (1). However, the limitations of the experimental techniques hitherto applied have precluded detailed analysis of this phenomenon. For our STEM data, the uncertainty implicit in any given mass determination is ~3%, whereas we observe an ~5-fold range of variation in molecular weights among purified BCV, and at least an 11-fold range among LCV. There is also considerable variation in shape. Although many CV are approximately spherical, others are distinctly ovoid (cf. Fig. 2) and we have observed ratios of longest/shortest dimension of up to 1.5. We do not think it likely that such prolate forms are imposed by distortion on preparation for electron microscopy because the major potentially distorting effect—adsorption to the carbon film—should not stress the particles anisotropically in this plane. The projected outer diameters, averaged over different directions, range from 50 to 100 nm for BCV and from 50 to 150 nm for LCV. Moreover, CV of a given diameter and shape can vary radically with respect to mass (Figs. 4 and 6), and the source of this variation evidently derives from the vesicular content rather than the coat. Although populations of BCV and LCV differ in the respects noted above (cf. Results), we have not detected any distinctive morphological differences between BCV and comparably sized LCV. The incidence of broken or incomplete particles is significantly higher among LCV, but this occurs predominantly among the larger particles that are not present among BCV.

Possible Functional Significance of CV Size Variation

In view of the diversity of functional roles attributed to CV, it seems probable that the collective population extracted from such a heterogeneous tissue source as brain should contain several functionally distinct types. On the other hand, liver, where the majority of cells are hepatocytes, is a considerably more homogeneous tissue. It is therefore noteworthy that isolated LCV exhibit a much wider variation in diameter and mass than BCV, and it is not unreasonable to inquire whether there may be some functional correlation to particular size classes. For instance, smaller CV might be expected to be more freely diffusible, and larger clathrin shells may transport correspondingly greater amounts of vesicular material.

Perhaps the most basic issue at this stage is to distinguish the extent to which these size variations represent the contributions of different cell types from the degree of variability in size that occurs within individual cells. Thus, Friend and Farquhar (3) found that CV in rat *vas deferens* cells are of two different size classes, are segregated to distinct compartments of the cytoplasm, and are engaged in different functions. More recently, Croze et al. (42, 43) have distinguished three size classes of CV in thin sections of mouse liver cells, which are associated primarily with the Golgi, the cytoplasmic membrane, and the intervening cytoplasm, respectively. It is perhaps premature to correlate these in situ observations conclusively with our analyses of isolated LCV, which demonstrate that the degree of heterogeneity in these populations is much greater than threefold. Nevertheless, these observations (3, 41, 42) indicate that CV particle size in certain cells does indeed correlate with proximity to specific types of membrane, and hence presumably with the CV-related activities in which the corresponding membranes are engaged.

APPENDIX

Linearity Range of Dark-field STEM Signal (Large-Angle Annular Detector)

The largest CV analyzed in this study have diameters of >150 nm and thus constitute relatively thick specimens. Motivated by this consideration, we have investigated the dynamic range over which the digital STEM signal can be taken as linear without incurring significant errors. Departures from linearity would be expressed in the mass determinations as systematic underestimates of total masses of individual

particles. This evaluation has been carried out empirically by analyzing images of latex beads, which are spheres of uniform density and are ~0.18 μm in diameter (Dow Uniform Latex Particles; E. F. Fullam, Schenectady, NY). For scattering from a chemically homogeneous specimen of linear density ρ, the dark-field signal (S_{DF}) is given by (36)

$$S_{DF}(t) = K(1 - \exp(-t/\lambda_e\rho), \quad (1)$$

where λ_e is the effective mean free path, t is the local mass thickness, and K is a proportionality constant. Let $t_e = \rho\lambda_e$ be the cumulative mass thickness to which this mean free path corresponds. Thus, for thin specimens, the linear approximation

$$S_{DF}(t) \sim \frac{K \cdot t}{t_e} \quad (2)$$

is adequate provided that t is restricted to small fractions of t_e. For elastic scattering of 40-keV electrons in amorphous carbon, λ_e has been estimated to be ~67 nm (36), which is equivalent to a value for t_e of 89 kdaltons. However, because the geometry of the large-angle detector may affect the value of this parameter, we have chosen to evaluate it empirically from scanned images of latex spheres. In these specimens, the projected mass thickness $t(x)$ as a function of position (x) is given by:

$$t(x) = c + 2\rho(r^2 - x^2)^{1/2} \quad \text{when} \quad |x| \leq r \quad (3a)$$

$$= c \quad \text{when} \quad |x| > r, \quad (3b)$$

where c is the mass thickness of the carbon film substrate, ρ is the linear density in latex, and r is the radius of a given sphere. This expression, in conjunction with Eq. 1, describes the dark-field signal in a scan across such a sphere and the parameters were evaluated by a nonlinear least-squares procedure (25). In Fig. 7, a typical fit is compared with the corresponding experimental signal and to the linear approximation (Eq. 2). Thus, we estimate $\lambda_e = 250 \pm 50$ nm for 40-keV electrons in latex for these operating conditions, which corresponds to an equivalent mass thickness of ~200 kdaltons.

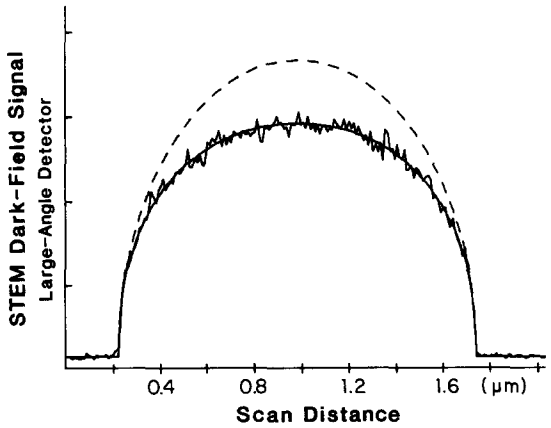

FIGURE 7 STEM dark-field signal recorded in scan across a latex sphere, approximately 0.16 microns in diameter. To improve the signal-to-noise ratio slightly, five scans were averaged to give this trace. The smoothly-varying solid line represents a fit to this curve given by Eqs. (1) and (3), whereas the dashed line represents the linear approximation of Eq. (2). The discrepancy between these curves indicates, at any point, the systematic departure from linearity caused by multiple scattering events.

To calculate quantitatively the effect of departures from linearity on the CV mass measurements, several STEM images were subjected to a nonlinear transformation, by inverting Eq. 1, viz.

$$t = t_e \ln\left[\frac{K}{K - S_{DF}}\right]. \quad (3)$$

For any given micrograph, this transformation depends on a single parameter, K, which must be determined. We evaluate K by applying Eq. 2 to the TMV particles that serve as our internal mass standards. Since for the maximal mass thickness presented by TMV in lateral projection, $t/t_e = 0.04$, and for the carbon support films used in these experiments, $\langle t/t_e \rangle$ ~0.017, the linear approximation clearly holds for these specimens.

The masses of a representative selection of CV particles were recalculated after this transformation, which compensates for the nonlinearities caused by multiple scattering events in the thicker parts of the specimen. Typical results are listed below:

Particle	Mass (linear approximation)	Mass (corrected)
	Mdaltons	*Mdaltons*
A	19.4	19.4
B	43.2	43.8
C	65.8	68.2
D	140.7	142.0
E	182.5	183.4

It is apparent that the discrepancies involved are slight in comparison with the overall experimental error attributed to these data (cf. Results). At first sight, this might seem paradoxical because the apparent diameters projected by large LCV (e.g., 150 nm) are still comparable to the empirically determined mean free path in latex, viz. 250 nm. However, it turns out that the total mass projected at any image point for such a CV is much smaller than at the corresponding point of a latex ball of the same thickness. This property may mean that there are substantial amounts of space within freeze-dried CV particles that are either empty or occupied by material of relatively low average density, or that these particles flatten to some extent on the electron microscope grid. At present we cannot distinguish between these two effects.

We gratefully acknowledge Dr. B. L. Trus for help in image processing, Dr. D. G. Tilley for film writing, Mr. M. Shapiro for advice on statistics, Drs. D. Thomas and S. Trachtenberg for helpful comments on the manuscript, and Ms. M. E. Quandt, Ms. K. Cheung, and Mr. F. Kito for expert technical assistance. We thank Ms. C. Cureton for preparing the manuscript.

Received for publication 7 March 1983, and in revised form 18 July 1983.

REFERENCES

1. Ockleford, C. D. 1981. Coated vesicles. *In* Electron Microscopy of Proteins. J. R. Harris, editor. Academic Press, Inc., London. 1:255–300.
2. Pearse, B. M. F., and M. S. Bretscher. 1981. Membrane recycling by coated vesicles. *Annu. Rev. Biochem.* 50:85–101.
3. Friend, D. S., and M. G. Farquhar. 1967. Functions of coated vesicles during protein

absorption in the rat vas deferens. *J. Cell Biol.* 35:357–376.
4. Ockleford, C. D., and A. Whyte. 1977. Differentiated regions of human placental cell surface associated with exchange of materials between maternal and foetal blood: coated vesicles. *J. Cell Sci.* 25:293–312.
5. Goldstein, J. L., R. G. W. Anderson, and M. S. Brown. 1979. Coated pits, coated vesicles and receptor mediated endocytosis. *Nature (Lond.).* 279:679–685.
6. Wall, D. A., and A. L. Hubbard. 1981. Galactose-specific recognition system of mammalian liver: receptor distribution on the hepatocyte cell surface. *J. Cell Biol.* 90:687–696.
7. Heuser, J. E., and T. S. Reese. 1973. Evidence for recycling of synaptic vesicle membrane during transmitter release at the frog neuromuscular junction. *J. Cell Biol.* 57:315–344.
8. Rothman, J., and R. Fine. 1980. Coated vesicles transport newly synthesized membrane glycoproteins from endoplasmic reticulum to plasma membrane in two successive stages. *Proc. Natl. Acad. Sci. USA.* 77:780–784.
9. Kanaseki, T., and K. Kadota. 1969. The vesicle in a basket. *J. Cell Biol.* 42:202–220.
10. Crowther, R. A., J. T. Finch, and B. M. F. Pearse. 1976. On the structure of coated vesicles. *J. Mol. Biol.* 103:785–798.
11. Heuser, J. 1980. Three-dimensional visualization of coated vesicle formation in fibroblasts. *J. Cell Biol.* 84:560–583.
12. Ungewickell, E., and D. Branton. 1981. Assembly units of clathrin coats. *Nature (Lond.).* 289:420–422.
13. Crowther, R. A., and B. M. F. Pearse. 1981. Assembly and packing of clathrin into coats. *J. Cell Biol.* 91:790–797.
14. Woods, J. W., M. P. Woodward, and T. F. Roth. 1978. Common features of coated vesicles from dissimilar tissues: composition and structure. *J. Cell Sci.* 30:87–97.
15. Pearse, B. M. F. 1976. Clathrin: a unique protein associated with intracellular transfer of membranes by coated vesicles. *Proc. Natl. Acad. Sci. USA.* 73:1255–1259.
16. Mello, R. J., M. S. Brown, J. L. Goldstein, and R. G. W. Anderson. 1980. LDL receptors in coated vesicles isolated from bovine adrenal cortex: binding sites unmasked by detergent treatment. *Cell.* 20:829–837.
17. Kellenberger, E., M. Häner, and M. Wurtz. 1982. The wrapping phenomenon in air-dried and negatively stained preparations. *Ultramicroscopy.* 9:139–150.
18. Steer, C. J., R. D. Klausner, and R. Blumenthal. 1982. Interaction of liver clathrin coat protein with lipid model membranes. *J. Biol. Chem.* 257:8533–8540.
19. Nandi, P. K., G. Irace, P. P. Van Iaarsveld, R. E. Lippoldt, and H. Edelhoch. 1982. Instability of coated vesicles in concentrated sucrose solutions. *Proc. Natl. Acad. Sci. USA.* 79:5881–5885.
20. Pearse, B. M. F. 1975. Coated vesicles from pig brain: purification and biochemical characterization. *J. Mol. Biol.* 97:93–98.
21. Laemmli, U. K. 1970. Cleavage of structural proteins during the assembly of the head of bacteriophage T_4. *Nature (Lond.).* 227:680–685.
22. Lowry, V. H., N. J. Rosebrough, A. L. Farr, and R. J. Randall. 1951. Protein measurement with the folin phenol reagent. *J. Biol. Chem.* 193:265–275.
23. McGee, P. A., B. L. Trus, and A. C. Steven. 1982. Techniques to evaluate the performance of scanning microdensitometers in the digitization of electron micrographs. *Micron.* 13:221–228.
24. Trus, B. L., and A. C. Steven. 1981. Digital image processing of electron micrographs—the PIC system. *Ultramicroscopy.* 6:383–386.
25. Knott, G. D. 1979. MLAB—a mathematical modeling tool. *Computer Programs in Biomedicine.* 10:271–280.
26. Fenner, C., R. R. Traut, D. T. Mason, and J. Wikman-Coffelt. 1975. Quantification of coomassie blue stained proteins in polyacrylamide based on analyses of eluted dye. *Anal. Biochem.* 63:595–602.
27. Wall, J. 1979. Mass measurements with the electron microscope. *In* Introduction to Analytical Electron Microscopy. J. J. Hren, J. I. Goldstein, and D. C. Joy, editors. Plenum Publishing Co., New York. 333–342.
28. Mosesson, M. W., J. Hainfeld, R. H. Haschemeyer, and J. Wall. 1981. Identification and mass analysis of human fibrinogen molecules and their domains by scanning transmission electron microscopy. *J. Mol. Biol.* 153:695–718.
29. Estis, J. F., and R. H. Haschemeyer. 1980. Electron microscopy of negatively stained and unstained fibrinogen. *Proc. Natl. Acad. Sci. USA.* 77:3139–3143.
30. Hainfeld, J. F., J. S. Wall, and E. J. Desmond. 1982. A small computer system for micrograph analysis. *Ultramicroscopy.* 8:263–270.
31. Steven, A. C., J. Wall, J. Hainfeld, and P. M. Steinert. 1982. Structure of fibroblastic intermediate filaments: analysis by scanning transmission electron microscopy. *Proc. Natl. Acad. Sci. USA.* 79:3101–3105.
32. Lindgren, B. W. 1968. Statistical Theory. Macmillan Science Co., Inc., Chicago. 329–332.
33. Lisanti, M. P., W. Schook, N. Moskowitz, C. Ores, and S. Puszkin. 1981. Brain clathrin and clathrin-associated proteins. *Biochem. J.* 201:297–304.
34. Lisanti, M. P., L. S. Shapiro, N. Moskowitz, E. L. Hua, S. Puszkin, and W. Schook. 1982. Isolation and preliminary characterization of clathrin-associated proteins. *Eur. J. Biochem.* 125:463–470.
35. Unanue, E. R., E. Ungewickell, and D. Branton. 1981. The binding of clathrin triskelions to membranes from coated vesicles. *Cell.* 26:439–446.
36. Crewe, A. V., and T. Groves. 1974. Thick specimens in the CEM and STEM. I. Contrast. *J. Appl. Phys.* 45:3662–3673.
37. Fertig, J., and H. Rose. 1977. A reflection on partial coherence in electron microscopy. *Ultramicroscopy.* 2:269–279.
38. Engel, A. 1978. Molecular weight determination by scanning transmission electron microscopy. *Ultramicroscopy.* 3:273–281.
39. Lamvik, M. K. 1978. Muscle thick filament mass measured by electron scattering. *J. Mol. Biol.* 122:55–68.
40. Woodward, M. P., and T. F. Roth. 1978. Coated vesicles: characterization, selective dissociation, and reassembly. *Proc. Natl. Acad. Sci. USA.* 75:4394–4398.
41. Mello, R. J., M. S. Brown, J. L. Goldstein, and R. G. W. Anderson. 1980. LDL receptors in coated vesicles isolated from bovine adrenal cortex: binding sites unmasked by detergent treatment. *Cell.* 20:829–837.
42. Croze, E. M., D. J. Morré, D. M. Morré, J. Kartenbeck, and W. W. Franke. 1982. Distribution of clathrin and spiny-coated vesicles on membranes within mature Golgi apparatus elements of mouse liver. *Eur. J. Cell Biol.* 28:130–138.
43. Croze, E. M., D. M. Morré, J. Kartenbeck, W. W. Franke, and D. J. Morré. 1982. Three size classes of spiny-(clathrin-) coated vesicles in rodent liver. *J. Cell Biol.* 95:429*a*. (Abstr.)
44. Harrison, P. M., G. A. Clegg, and K. May. 1980. Ferritin structure and function *In* Iron in Biochemistry and Medicine. A. Jacobs and M. Worwood editors. Academic Press, Inc. London. 2:131–172.